# A Technique for Standardized Central Analysis of 6-$^{18}$F-Fluoro-L-DOPA PET Data from a Multicenter Study

Alan L. Whone, MRCP[1]; Dale L. Bailey, PhD[2]; Philippe Remy, PhD[3]; Nicola Pavese, MD[1]; and David J. Brooks, DSc[1]

*[1]Division of Neuroscience and MRC Clinical Sciences Centre, Faculty of Medicine, Imperial College, Hammersmith Hospital, London, United Kingdom; [2]Department of Nuclear Medicine, Royal North Shore Hospital, Sydney, Australia; and [3]CEA-Centre National de la Recherche Scientifique Unité de Recherche Associée 2210, Service Hospitalier Frederic Joliot, Orsay, France*

We have recently completed a large 6-$^{18}$F-fluoro-L-DOPA ($^{18}$F-DOPA) PET study comparing rates of loss of dopamine terminal function in Parkinson's disease (PD) patients taking either the dopamine agonist ropinirole or L-DOPA. This trial involved a "distributed acquisition/centralized analysis" method, in which $^{18}$F-DOPA images were acquired at 6 different PET centers around the world and then analyzed at a single site. To our knowledge, this is the first time such a centralized approach has been employed with $^{18}$F-DOPA PET and this descriptive basic science article outlines the methods used. **Methods:** One hundred eighty-six PD patients were randomized (1:1) to ropinirole or L-DOPA therapy, and $^{18}$F-DOPA PET was performed at baseline and again at 2 y. The primary outcome measure was the percentage change in putamen $^{18}$F-DOPA influx rate constant ($K_i$) from Patlak graphical analysis. Dynamic images were acquired and reconstructed using each center's individual protocols before being transferred to the site performing the central analysis. Once there, individual parametric $K_i$ images were created using a single analysis program without file formats being transformed from the original. Parametric images were then normalized to standard space and $K_i$ values extracted with a region of interest analysis. Significant $K_i$ changes were also localized at a voxel level with statistical parametric mapping. These processes required numerous checks to ensure the integrity of each dataset. **Results:** Three hundred twenty-five (170 baseline, 155 follow-up) dynamic PET datasets were acquired, of which 12 were considered uninterpretable due to missing time frames, radiopharmaceutical problems, lack of measured attenuation correction, or excessive head movement. In those datasets suitable for central analysis, after quality control and spatial normalization of the images had been applied, putamen $^{18}$F-DOPA signal decline was found to be significantly (one third) slower in the ropinirole group compared with that of the L-DOPA group. **Conclusion:** Paired $^{18}$F-DOPA-PET images acquired from multiple sites can be successfully analyzed centrally to assess the efficacy of potential disease-modifying therapies in PD. However, numerous options must be considered and data checks put in place before adopting such an approach. Centralized analysis offers the potential for improved detection of outcomes due to the standardization of the analytic approach and allows the analysis of large numbers of PET studies.

**Key Words:** PET; $^{18}$F-DOPA; Parkinson's disease; progression; central analysis

**J Nucl Med 2004; 45:1135–1145**

With rapid advances in molecular medicine, the production of neuroprotective or neurorestorative agents that affect the progression of degenerative conditions such as Parkinson's disease (PD) is becoming a realizable ambition for academic institutions and pharmaceutical companies. That said, although the safety and tolerability of novel agents can often be confirmed in a straightforward manner, demonstrating therapeutic efficacy is frequently more complex (*1*,*2*). The gold standard for assessing in vivo drug benefit is the analysis of clinical outcome measures after double-blind randomized controlled clinical trials. However, assessing disease-modifying therapies in PD by clinical outcome measures alone may be problematic (*1*,*2*). Hence, besides the need for the development of neuroprotective treatments in PD, there is a requirement for the development of adjunctive objective measures by which therapeutic efficacy can be assessed. In this regard, 6-$^{18}$F-fluoro-L-DOPA ($^{18}$F-DOPA) PET has been shown to provide an objective biomarker of PD progression, where the fall in striatal $^{18}$F-DOPA PET uptake over time reflects the degeneration of dopamine terminals (*3*–*5*).

We have recently completed a randomized controlled clinical trial assessing, in early PD, the potential disease-modifying effects of ropinirole, a dopamine agonist, compared against L-DOPA treatment where changes in $^{18}$F-DOPA PET signal rather than clinical endpoints were the primary outcome measure and where statistically significant differences in $^{18}$F-DOPA uptake loss were found (*6*). This investigation obtained effect sizes similar to 2 previous $^{18}$F-DOPA studies investigating dopamine agonists in PD

Received Sep. 8, 2003; revision accepted Jan. 14, 2004.
For correspondence or reprints contact: Alan L. Whone, MRCP, Cyclotron Building, Hammersmith Hospital, Du Cane Rd., London, W12 0NN, U.K.
E-mail: alan.whone@csc.mrc.ac.uk

(*7,8*) but involved group sizes far larger than reported previously (enrolled population = 186). To study such a large population at a single PET site would be a considerable undertaking and have major implications in terms of patient recruitment and retention. Thus, a "distributed acquisition/centralized analysis" model was used, in which data were acquired at 6 different PET centers around the world and then analyzed in a standardized manner at a single site. The clinical and imaging results of this study have been reported elsewhere (*6*); therefore, the purpose of this descriptive methodologic paper is to provide further details of our method of centralized PET analysis. To our knowledge, this is the first study of PD progression to utilize a centralized analysis technique, and this article outlines the methodology used to organize, implement quality control, and standardize such a large volume of image datasets (170 baseline scans, 155 follow-up scans) emanating from different PET centers. It is hoped this will serve as a guide for similar studies in the future.

## MATERIALS AND METHODS

### Study Design and Subjects

We used a standard method for assessing $^{18}$F-DOPA uptake, in which it is assumed there is monodirectional uptake from the blood into the basal ganglia, via the exchangeable pool, after injection of the radiotracer. The Patlak graphical analysis technique (*9,10*) applied to such a system allows the derivation of an influx rate constant ($K_i$), which measures the rate of accumulation of the radiotracer.

One hundred eighty-six patients with a clinical diagnosis of PD and symptom duration of ≤2 y were assigned (1:1) to ropinirole or L-DOPA therapy by the sponsor. $^{18}$F-DOPA PET was performed between 4 wk and 3 mo after drug initiation and again at 2 y (within 4 wk of the 24-mo clinical assessment). The primary outcome measure was the mean percentage reduction in the side-to-side averaged putamen $^{18}$F-DOPA influx constant ($K_i$) between pairs of baseline and follow-up scans. $^{18}$F-DOPA PET imaging was performed at 6 centers in Europe and North America (Table 1) with all dynamic image sequences forwarded to our center for analysis. As the purpose of this article is to describe how we performed this distributed acquisition/centralized analysis, details of power calculations, patient selection criteria, blinding, randomization, clinical assessment, drug dosing, baseline demographics, and patient withdrawal are not reported here but can be found in the article describing the primary study outcomes (*6*).

### PET Cameras

The 6 PET cameras used are shown in Table 1. Siemens/CTI manufactured all of the cameras; however, a variety of models were used. It was recognized that investigating a combination of images from different tomographs, each with different resolution and sensitivity, could introduce bias. However, the study protocol stipulated baseline and follow-up scans be acquired with the same camera and the outcome measure was the percentage (rather than absolute) change in putamen $K_i$ between scan pairs. It was also acknowledged there was a risk of bias if more patients from one



**TABLE 1**
Details of PET Centers, Scanners Used, Acquisition Protocol, and Subject Numbers

| PET center | Scanner model | Reported in-plane spatial resolution: FWHM (mm) | Reported in-plane spatial resolution: Reference | Acquisition protocol (frame sequence) | No. of subjects in study* |
|---|---|---|---|---|---|
| United Kingdom Hammersmith | ECAT HR++ | 4.5 | 11 | 26 frames; higher frame frequency acquisition initially, 95-min duration | 34 baseline scans: 16 r, 18 l<br>Outcome population: 12 r, 12 l |
| France Orsay | ECAT HR+ | 4.6 | 12 | 9 frames; frame frequency acquisition constant throughout, 90-min duration | 39 baseline scans: 19 r, 20 l<br>Outcome population: 17 r, 16 l |
| United States Atlanta | ECAT EXACT47 | 6.0 | 13 | 29 frames; higher frame frequency acquisition initially, 120-min duration | 39 baseline scans: 19 r, 18 l<br>Outcome population: 15 r, 11 l |
| Germany Ulm | ECAT EXACT47 | 6.0 | 13 | 9 frames; frame frequency acquisition constant throughout, 90-min duration | 25 baseline scans: 15 r, 10 l<br>Outcome population: 10 r, 6 l |
| Canada UBC | ECAT 953B | 4.8 | 14 | 25 frames; higher frame frequency acquisition initially, 95-min duration | 20 baseline scans; 11 r, 9 l<br>Outcome population: 10 r, 7 l |
| Canada McMaster | ECAT ART | 6.2 | 15 | 58 frames; frame frequency acquisition constant throughout, 150-min duration | 15 baseline scans; 5 r, 10 l<br>Outcome population: 4 r, 7 l |

*Subjects undergoing baseline scans at each center and subjects from each center in primary outcome population (after patient withdrawals).

FWHM = full width at half maximum; r = ropinirole; l = L-DOPA; UBC = University of British Columbia.

Data format versions used for each scanner were CTI proprietary formats, either ECAT6 or ECAT7.

treatment group underwent imaging with lower resolution tomographs compared with the other. In such a situation, there may have been less sensitivity to detect longitudinal change in one group. To reduce this confound, a stratified randomization was used with similar numbers allocated to ropinirole or L-DOPA within each center (Table 1). Data were analyzed blind to treatment but after unblinding, it was confirmed centers had scanned similar numbers receiving either treatment and this similarity remained after withdrawals (Table 1). This equal distribution of treatment types between centers was also pertinent because of the different acquisition and reconstruction protocols used by each site, also recognized as sources of potential bias.

### Data Acquisition

All patients stopped dopaminergic medication 12 h before imaging. Twelve hours is the usual time length for omitting dopaminergic agents before scanning and exceeds plasma half-life several fold. There is no direct evidence that agents acutely effect $^{18}$F-DOPA uptake (*16*,*17*); however, over the longer term this is less clear (see results discussion). To improve $^{18}$F-DOPA availability to the brain, all patients were pretreated with 150 mg of carbidopa and 400 mg of the catechol-*O*-methyltransferase (COMT) inhibitor entacapone 1 h before scanning, improving the signal-to-noise ratio (*18*,*19*). Giving entacapone was not the usual practice of some of the PET centers involved. $^{18}$F-DOPA was synthesized in each center's usual way and 150–180 MBq were administered as an intravenous bolus at the start of dynamic acquisition. The dose administered was determined by the standard practice at each site but was required to be consistent between scan pairs and for all scans at each center. To achieve cooperation between centers and to ensure the quality and reproducibility of acquired data, it was deemed appropriate to allow centers to acquire dynamic images, as much as possible, in their standard manner. Therefore, centers followed their usual $^{18}$F-DOPA acquisition protocols with as few central specifications as possible. However, centers were instructed to use the same acquisition method for each patient scanned at their site, collect all data in 3-dimensional (3D) mode (*20*), start acquisition of the dynamic data from the time of radiotracer injection, and collect the entire time series for at least 90 min. The number of frames acquired and their duration was not stipulated, and centers were permitted to collect data beyond 90 min, though these additional data points were not used in the central analysis (Table 1).

### Image Reconstruction

Image reconstruction was performed at each center using the standard manufacturer-supplied 3D reconstruction program provided with their respective PET cameras. Various choices can be made within this reconstruction program (e.g., filter window used, zoom factor, whether to decay correct, and so forth), and each site used their preferred method. Five of the 6 centers corrected for attenuation using a measured transmission scan, acquired before dynamic acquisition, whereas one center used a calculated attenuation correction for both baseline and follow-up images. Although the reconstruction procedure was not defined in the protocol, all centers used the fully 3D reprojection filtered backprojection algorithm (*21*), and scatter correction was applied during the reconstruction process using the single scatter model (*22*,*23*). Detector normalization and geometric corrections were applied using the scanner manufacturer's standard methods.

### File Formats and Data Transfer

An important logistic issue in a study such as this is that an appropriate format for image data files be used. Although rarely discussed, file format incompatibilities can severely restrict the ability to transfer data between centers. This is being addressed now with the introduction of the Digital Imaging and Communications in Medicine (DICOM) standard; however, complete support for PET data on different platforms is still not fully deployed.

The software file format used in the study was the "matrix" format, which is used by the scanner manufacturer CTI. This format is data rich and the header information includes parameters such as the method of attenuation and scatter correction, decay correction flags, normalization information, frame timing information, and reconstruction parameters as well as the standard, required information of matrix dimensions, pixel size, and so forth. Not requiring centers to translate file formats reduced the potential for errors as the central site accepted data that did not require any conversion, exporting, or processing.

After local reconstruction of dynamic files, data were copied to CD-ROM to allow transfer to Hammersmith, which was the site chosen to perform the central analysis based on having validated, published analysis software for 3D $^{18}$F-DOPA PET (*24*). The point-to-point file transfer protocol ftp was not used due to the large sizes of some of the files (>80 Mbytes per scan).

Before transferring all studies, each center sent 3 pilot baseline and follow-up scans to verify compatibility of their reconstructed images with our programs for analysis. During this verification process several problems were identified. It was discovered that one center routinely reoriented images to the anterior commissure–posterior commissure (AC–PC) line after reconstruction and that another center had used a calculated attenuation correction for some of their first PET scans and a measured attenuation correction for their second PET scans. The center that had performed realignment was asked to provide images in native orientation. It was believed this was important, as otherwise the images from this center would have undergone more spatial transformations and manipulations (with associated interpolation). The center that used a different attenuation method for some of their first and second scans was asked to provide both images using a calculated attenuation correction.

After receiving the reconstructed images, a validity check was performed on each dataset. This included verifying that all time frames were present, that the duration was ≥90 min, that the data had been corrected for attenuation and scatter, and that normalization had been applied for detector differences and geometric effects. During this process, 5 scans were identified as not containing some of their time frames; therefore, these scans were excluded from the study (Table 2).

### Creation of Parametric Images

Once the integrity of the dynamic time series had been verified, parametric images of specific $^{18}$F-DOPA influx constant ($K_i$ maps) were created on a voxel-wise basis for the whole brain, using Patlak graphical analysis (*9*,*10*) with an input function derived from a reference region, the occipital cortex (*25*). Using the reference region method, no extra data—apart from the dynamic images—were required. Occipital cortex, rather than cerebellum, which has been used in other $^{18}$F-DOPA PET investigations from our center (*26*), was chosen as the reference region as some of the cameras used had a limited axial field of view and were restricted in the degree of cerebellar volume included in their basal ganglia

**TABLE 2**
Number of Scans Identified and Removed Because of Particular Problems

| Reason for rejecting scan | Baseline PET | Follow-Up PET |
|---|---|---|
| Scans identified from subjects considered to be unevaluable | | |
| Incomplete frame sequence | 2 | 3 |
| Input function suggestive of poor radiotracer delivery/status | 1 | 2 |
| Attenuation correction not applied | 0 | 1 |
| Abnormal input function suggestive of excessive head movement | 1 | 1 |
| Gross misalignment between ADD and $K_i$ images suggestive of excessive head movement | 0 | 1 |
| Scans identified from baseline subjects who subsequently withdrew considered to be unevaluable | | |
| Dynamic image not sent | 2 | |
| Scans identified as problematic and data resent from local center | | |
| Wrong scan contained on CD-ROM | 0 | 1 |
| Attenuation correction not applied | 1 | 0 |
| Scans not contained on CD-ROM | 2 | 2 |

In addition, 1 center was asked to send all datasets using the same attenuation correction method for both baseline and follow-up scans; another center was asked to send their images in native space only and not reorientated to AC–PC line.

investigations. It was recognized that the same reference tissue should be used in every case. The software used to create the parametric images was developed in-house in IDL (Interactive Data Language; Research Systems International) and has been validated previously (*24*). One feature to emphasize with this method is that the only dataset required for full analysis is the reconstructed dynamic image series, greatly simplifying data management. Because we used software developed in-house by one of the investigators, adaptations of the program to accommodate data sent from different centers could be made, allowing all data to be processed using the same analysis package. The net influx rate constant ($K_i$) was calculated over the range 30–90 min for each pixel individually; therefore, files that contained time frames after the 90-min time point were truncated to increase conformity. The used outputs of this program were a parametric whole brain volume showing the net influx rate constant ($K_i$; units: $mL \cdot min^{-1} \cdot g^{-1}$) and an image of integrated $^{18}$F-DOPA signal from 30 to 90 min (an "ADD" or summed image) (Fig. 1). The ADD image was subsequently used during spatial normalization of the individuals $K_i$ map to an $^{18}$F-DOPA template (see below).

Checks on the integrity of each $K_i$ map and ADD image were then performed. First, the input function for each scan was reviewed. Typical input function curves are shown in Figures 2A and 2D and demonstrate occipital cortex time–activity curves with fast radiotracer uptake and then washout, indicating a lack of specific binding. However, in several cases, the appearance of the curve was different. The differences seemed to fall into 2 types: one was the appearance of a jagged curve (Fig. 2C), which we believed most likely represented excessive head movement; and the second were input curves demonstrating very low radiotracer activity (Fig. 2B), which we believed indicated either poor radiopharmaceutical synthesis, breakdown, or decay before injection or poor intravenous administration (extravasation). Because it was recognized that aberrant input functions could render $K_i$ values uninterpretable, the few scans in which these problems were observed were excluded (Table 2).

The next check was an interactive visual assessment of the appearance of each transverse section of the ADD and $K_i$ images, which was performed using Analyze software (Analyze AVW; Mayo Clinic). From experience, we have observed that untransformed ADD and $K_i$ images produced from the dynamic time series are not always in alignment. This becomes problematic later when using the ADD image to achieve spatial normalization of the $K_i$ map. Our investigations have revealed that relative spatial shifts between ADD and $K_i$ images reflect head movement between early and late time frames. The explanation is that the $K_i$ image is weighted to later time points, whereas the ADD image is weighted toward earlier time points when head counts are highest. Therefore, head movement toward the end of the scan has a greater effect on the $K_i$ map than on the ADD image. In cases in which a mismatch between the ADD image and the $K_i$ map orientation was evident, this was noted for consideration during the blind regions of interest (ROI) $K_i$ extraction (see below). When this relative shift was severe, the entire dynamic sequence was reevaluated and the data were excluded (Table 2) if head movement was believed to be excessive (exclusion occurred if there was gross misalignment,

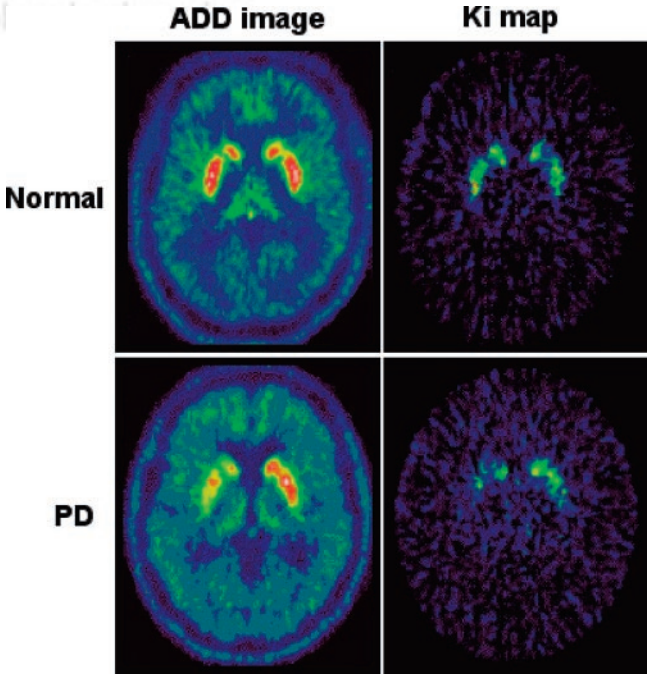


**FIGURE 1.** ADD (summed) and net influx rate constant ($K_i$) maps of single slice from healthy subject (top) and subject with PD (bottom). In these images, normalization to Montreal Neurological Institute (MNI) space has been performed. High signal, demonstrating high $^{18}$F-DOPA uptake, is shown in red bilaterally in caudate nucleus and putamen. In subject with PD, there is reduction of uptake in caudate and putamen that is greater on right-hand side.

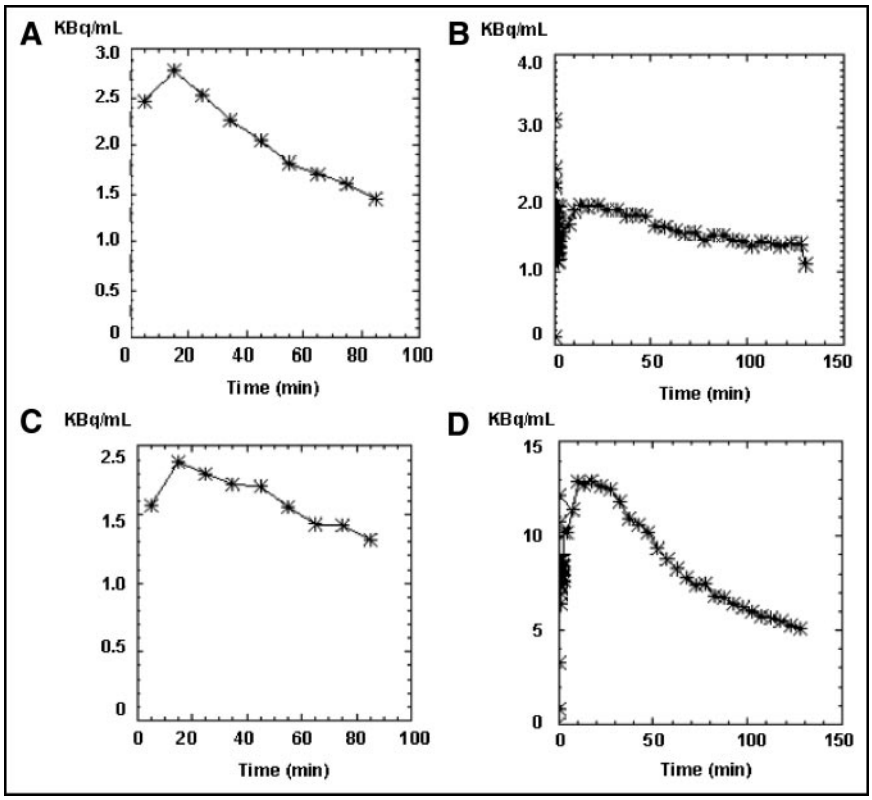


**FIGURE 2.** Four input function curves are shown from 2 subjects, (A + C) and (B + D). Input curves (A + B) are from baseline scans and input curves (C + D) are from follow-up scans. (A + D) input function curves are within normal acceptable limits. C is an example of a jagged input function curve, suggesting excessive head movement during scan. B is an example of a flat input function curve, suggesting either poor radiotracer delivery or decay before injection. In B (baseline scan), peak is factor of 10 lower than in D (follow-up scan). Both subjects (A + C) and (B + D) were excluded from analysis on basis of these aberrant curves (C + B).

particularly in the *z*-axis, which could not be remedied by manual adjustment of the object map—see below).

### Spatial Normalization of Parametric Images and ROI Analysis

One step toward minimizing the number of variations in this study was standardization of the ROIs applied to the datasets. This was done using a single template of predefined volumes of interest and applying these to each spatially transformed parametric image. We perceived several advantages in placing ROIs on spatially transformed rather than native space parametric images. First, the method allowed the same cubic volume to be interrogated in all scans. Second, by normalizing each parametric image to the same orientation and space, we increased our confidence that we were assessing the same subregion of putamenal tissue in both baseline and follow-up images. This is important when assessing PD progression because putamen dopamine terminal loss is not homogeneous (*27*). Rather, there is a subregional pattern of terminal decline, previously demonstrated with $^{18}$F-DOPA PET, with greater $K_i$ loss in the dorsal caudal putamen in early PD (*26*,*28*). Therefore, if the region interrogated in the follow-up study was defined more ventrally and rostrally than in the baseline study, the apparent fall in $K_i$ would be underestimated. Conversely, if the region in the follow-up study was placed more dorsally and caudally, the apparent fall would be exaggerated. With the advent of high-resolution 3D PET, ROI placement differences can have a large effect and considering this when assessing longitudinal change is critical.

To effect spatial normalization, we used the spatial normalization algorithm available in statistical parametric mapping, SPM99 (*29*). This process transformed each individual $K_i$ image into standard spatial coordinates known as the Montreal Neurological Institute (MNI) space, which is the same space as the MRI templates in SPM99 (Table 3.1).

Having transformed the ADD, and, subsequently, the $K_i$ images to standard space, the volumes-of-interest template (object map) was applied (Fig. 3). The object map defined both putamen, heads of caudate nuclei, and ventral striatum. ROI objects were drawn freehand on the MNI single-subject MRI (*26*,*30*) found in SPM99 by an expert neuroanatomist. Visual inspection of each normalized plane of both $K_i$ and ADD images was then made to ensure correct placement of the template region over the structure, where normalized ADD images were used to guide anatomic placement. If misalignment of the template ROI and the $K_i$ map target region was seen, the ROI was moved to overlie the structure. Such misalignment occurred most commonly in the *x*-plane and required movement within the transaxial slice. Misalignment was seen most frequently over the caudate nucleus (Fig. 4), presumably in part due to the relatively small volume of this structure in the *x*-plane. Where this had occurred it was invariably due to head movement, causing the above-mentioned misalignment between the native ADD and $K_i$ image, which was then exacerbated after spatial normalization (Fig. 4). Although moving the target regions by hand may seem to negate the purpose of this seemingly automated object placement approach, the maneuver was necessary, as a small misalignment can have a profound effect due to the disparity between high uptake in the striatum compared with that of the surrounding white matter. The volume of the ROIs was maintained in this action and adjustments were performed blind to treatment. Further to the above, it was noted that the amount of correction required varied between centers and probably reflected the degree of head movement permitted by different head restraint systems. Predominantly, ROI $K_i$ data were collected concurrently for each

**TABLE 3**
SPM Settings

| Setting | Procedure |
|---|---|
| 3.1 | SPM settings and procedures used to effect spatial normalization |
| A | SPM defaults were set so that bounding box was same as MNI MRI templates found in SPM99 and orientation changed to radiologic convention. |
| B | Individual ADD images were normalized to $^{18}$F-DOPA template created in-house in MNI space (ADD images were used for this iterative maneuver as ADD images contain information reflecting cerebral blood flow and nonspecific binding and, therefore, have greater anatomic detail than $K_i$ maps.). |
| C | Having normalized ADD images to MNI space, $K_i$ maps were normalized by applying ADD image transformation parameters (This is problematic if native space ADD and $K_i$ images are not in alignment.). |
| D | Normalization quality was inspected in SPM99, comparing spatially normalized $K_i$ and ADD images with $^{18}$F-DOPA template and MNI single-subject MRI. |
| 3.2 | SPM settings used when performing within-group and between-group analysis |
| A | Subjects were entered into SPM such that baseline and follow-up smoothed normalized $K_i$ maps were conditions 1 and 2, respectively. |
| B | There were no covariates and SPM options were set to no global normalization, no nuisance variables, and no grand mean scalings. |
| C | Analysis lower threshold was set to zero and upper threshold to absolute. By choosing these options, it was variance in voxel-by-voxel $K_i$ values that were being compared, rather than differences in scaled or proportional values. |

ADD image in this case is summed image of integrated $^{18}$F-DOPA signal from 30 to 90 min; MRI is magnetic resonance image.

subject's baseline and follow-up PET scan, so differences in the image quality between the first and second scans as well as differences in the quality of normalization could be recorded. After collection of all results, the $K_i$ database was locked. Statistical tests on the ROI data were then performed by the sponsor's statisticians using predefined statistical tests (*6*).

During blind ROI analysis of the baseline PET data acquired at our center (Hammersmith), which was analyzed first (ahead of follow-up analysis), it was seen that 5 of 34 (15%) subjects had normal baseline PET imaging. As the primary endpoint of the trial was relative rates of decline in putamen $K_i$, we were concerned that if in these subjects follow-up imaging showed no decrease in $^{18}$F-DOPA uptake and if this level of discordance (15%) between clinical diagnosis and PET findings was seen across all centers, at our given statistical power, the outcome measure would be biased if more subjects with "normal" PET scans by chance fell into one treatment group or another. Consequently, an investigator meeting was held midstudy and it was decided that subjects with normal baseline PET should be excluded a priori from our primary outcome measure—that is, before closure of the $K_i$ database and statistical analysis. This approach has recently been proposed by another group performing similar trials using SPECT (*31*). After collecting all ROI data but before unblinding, or the application of statistical tests, the baseline $K_i$ results were reviewed independently by 3 investigators and 21 of 183 subjects were identified as having normal baseline scans and excluded. Further information on the PET findings of these subjects is given in the original article (*6*), and a further clinical investigation into these subjects is ongoing.

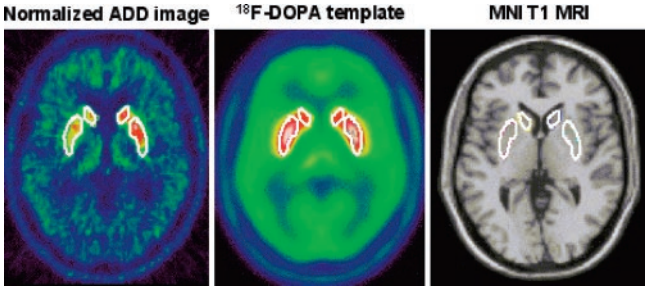


**FIGURE 3.** Template region object map (white outlines) overlying putamen and caudate nucleus bilaterally in normalized ADD (summed) image, $^{18}$F-DOPA template, and single subject T1 MRI found in SPM99.

## SPM

The spatially normalized parametric $K_i$ maps were also analyzed using SPM software (*32–35*). After the application of an

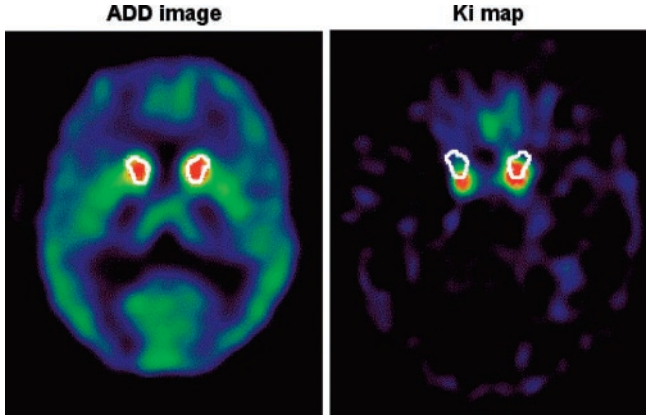


**FIGURE 4.** Example of poor alignment between ADD (summed) and $K_i$ image in *x*-axis at level of caudate nucleus (red). Consequently, object map (white circles) is correctly localized in ADD image but not in $K_i$ map. In this situation, manual adjustment would be made so that object map (white circles) would lie over caudate nucleus (red) in $K_i$ map before $K_i$ values are extracted.

8-mm smoothness parameter (full width at half maximum) (*36*), paired comparisons were made to localize significant mean $K_i$ differences between baseline and follow-up scans within and between treatment groups. To do this it was necessary to categorize subjects into treatment groups; hence, partial unblinding of the treatment arms was required. This information was not made available until 3 wk after the central ROI $K_i$ database was closed. We remained unaware of which group had received each medication, simply categorizing the groups X and Y. The whole brain volume was first investigated to identify peak voxels of significant $K_i$ change between baseline and follow-up within each group (Table 3 shows SPM settings), where the significance threshold was set to $P = 0.005$ (cluster size = 100 voxels). To estimate the magnitude of change, individual $K_i$ values from SPM-identified peak voxels of change were extracted and the results were sent to the study statistician to undergo predefined statistical tests (*6*).

SPM was also used to localize voxels of significant relative differences in rates of mean $K_i$ loss between the 2 groups ($\{\text{baseline}[K_i] - \text{follow-up}[K_i]\}_X - \{\text{baseline}[K_i] - \text{follow-up}[K_i]\}_Y$) and vice versa, where X is one treatment group and Y the other (extent threshold, $P = 0.05$; cluster size, 10 voxels). Because the within-group comparison had only identified significant changes within the striatum and midbrain in either group, a cortical mask was applied, removing comparisons within the cortex and, therefore, reducing the level of correction required.

### Local ROI Analysis

At the start of the study all 6 PET centers were invited to analyze their data in a blind fashion, locally, and to derive influx rate constants ($K_i$) for the putamen and caudate. Each center performed an ROI assessment using their usual technique and, accordingly, 6 different methods were used (including defining standard size volumes on native space ADD images or placing regions on PET images coregisterd to individual MRI). None of these local analyses used spatial normalization. The methodology for performing a centralized analysis with spatial normalization was developed during the course of this multiyear trial. Once this methodology was available, it was determined ahead of analysis that a centralized approach would provide the primary imaging endpoint. However, the local analysis regional $K_i$ data were recorded and collected by the study statistician. As with the central analysis, after collection of all local $K_i$ data, the database was locked and predefined statistical tests applied. Both central and local $K_i$ databases were locked simultaneously, so the results of one analysis were not known ahead of another. Furthermore, the local $K_i$ data from the 5 remote PET centers were not available to the center performing the central analysis. Before locking the database and performing statistical evaluation, it was decided to remove the local $K_i$ data from the 21 subjects identified in the central analysis as having normal baseline imaging.

## RESULTS

Results of baseline and endpoint clinical status and the primary outcome measures of the ROI and SPM analyses have already been reported (*6*). Therefore, the results detailed here are as follows: (a) summary statistics pertinent to understanding the utility of our distributed acquisition/centralized analysis approach; (b) a brief report of the PET primary outcome findings; (c) unreported data from ROI analyses of the caudate nucleus and ventral striatum; and (d) the results of the local ROI analysis. The data from the caudate nucleus and ventral striatum along with PET data from the baseline and follow-up subjects with normal baseline imaging are presented here as it is recognized that the 2 therapies may have directly and differentially affected $^{18}$F-DOPA uptake independent of the effects on disease progression (*37*). Presenting these data goes some way in addressing this issue.

Of 186 randomized patients, 3 did not receive study medication (3/186; 1.6%). Of the 183 remaining patients, 13 withdrew before their initial PET scan (4–12 wk after drug initiation) (13/186; 7%). Hence, a total of 170 baseline PET images were acquired at the 6 PET centers involved (Table 1). Of these, 2 were not forwarded to our center (both from subjects who subsequently withdrew before follow-up PET) and 4 were considered uninterpretable (Table 2). Therefore, 164 of 186 (88.2%) randomized patients had an analyzable baseline PET scan. Of the 164 analyzable baseline scans, 21 (12.8%, 19 of whom underwent follow-up PET) were considered to be normal. One hundred fifty-five of the 170 (92%) subjects who underwent baseline PET had follow-up imaging, including subjects withdrawing from the trial after 1 y, who were asked to undergo follow-up PET at the point of withdrawal and were included in the primary outcome measure. Eight of 155 (5.2%) of the follow-up PET datasets were considered uninterpretable, where 3 of 8 of these subjects also had nonevaluable baseline imaging (Table 2). Therefore, of the 155 follow-up (paired) PET datasets—after removal of 19 of 21 subjects with paired normal baseline imaging (19/155; 12.3%) and 9 subjects without analyzable pairs of scans (9/155; 6%) (Table 2)—127 paired (68 ropinirole, 59 L-DOPA) $^{18}$F-DOPA images remained for assessment of the primary outcome measure (127/186; 68.3%) (mean scan-to-scan interval: ropinirole, 615 ± 97.7 d; L-DOPA, 613 ±103.3 d).

The results of the PET primary outcome findings given here are provided in more detail in the original publication (*6*). The template ROI analysis performed on spatially normalized $K_i$ maps showed a significantly smaller reduction ($P = 0.022$) in putamen $K_i$ in the ropinirole group (−13.4%) compared with the L-DOPA group (−20.3%; 95% confidence interval [CI]: 0.65, 13.06), with an absolute difference of 6.86% in putamen percentage $K_i$ reduction between the 2 groups and an SD of 16.5%. The within-group SPM analysis demonstrated less extensive reduction in putamen $K_i$ ($P < 0.005$ threshold; cluster size, 100 voxels) and substantia nigra $K_i$ with ropinirole compared with L-DOPA. Voxels of the most significant $K_i$ decrease within each group were localized bilaterally in the putamen, and a comparison of magnitude of change in putamen voxels of peak significance showed a significant relative difference in favor of ropinirole (38%; $P < 0.001$). The between-group SPM ("difference of the differences") showed 2 regions of significantly greater $K_i$ loss in the L-DOPA group compared with the ropinirole group (posterior dorsal putamen and substantia nigra bilaterally),

whereas there were no regions of greater $K_i$ loss in the ropinirole group compared with the L-DOPA group ($P < 0.05$ threshold; cluster size, 10 voxels).

In addition to the putamen, 2 further striatal regions were outlined on the template object map, caudate nucleus and ventral striatum. The total patient (L-DOPA group and ropinirole group) mean progression in the caudate nucleus (−12.6%) was significantly less than that in the putamen (−16.8%) (relative difference putamen vs. caudate, 25.0%; $P = 0.0001$ [paired 2-tailed t test]). There was a trend toward slower progression in the caudate nucleus in the ropinirole group compared with the L-DOPA group (ropinirole, 10.0%; L-DOPA, 14.6%; $P = 0.08$). The total patient mean progression in the ventral striatum (−9.6%) was significantly less than that in either the putamen (−16.8%) or the caudate nucleus (−12.6%) (relative difference putamen vs. ventral striatum, 42.9%, $P = 0.000001$; relative difference caudate vs. ventral striatum, 23.8%, $P = 0.05$). Little difference was seen in the ventral striatal rate of progression between the ropinirole and the L-DOPA group (ropinirole, 8.71%; L-DOPA, 9.99%; $P$ = not significant) (Table 4). Compared with a Hammersmith database of 16 healthy control subjects (*11*), the total patient baseline putamen $K_i$ mean ± SD (0.0086 ± 0.0023) was 3.8 SDs below that of control subjects (0.0150 ± 0.0017). The total patient mean baseline caudate $K_i$ (0.0120 ± 0.0017) was 1.3 SDs below that of control subjects (0.0142 ± 0.0017) and the mean baseline ventral striatum $K_i$ (0.0128 ± 0.0027) was similar to that of control subjects (0.00127 ± 0.0013).

The local ROI analysis of spatially nonnormalized putamenal $^{18}$F-DOPA uptake rate showed no significant difference in loss of $K_i$ with ropinirole (−15% ropinirole vs. −18% L-DOPA) ($P = 0.354$; −95% CI: −3.13, 8.68). Although the 19 pairs of scans identified as normal in the central analysis were removed before running the local analysis, 8 of 9 of the pairs of scans identified as being unevaluable in the central analysis were included. This was because data from these scans had been provided by the local centers, where, presumably, the concerns regarding these scans had either not been identified or considered insufficient to warrant exclusion. The $K_i$ values from the images lacking some time frames were within the expected range; however, the scans that were identified as having poor radiotracer synthesis or delivery did indeed have spuriously low $K_i$ values. The total patient mean putamen baseline and follow-up $K_i$ values were similar with the central and local ROI approaches, as were the SDs of the means (central analysis baseline $K_i$, 0.0086 ± 0.0023; local analysis baseline $K_i$, 0.0084 ± 0.0022; central analysis follow-up $K_i$, 0.0069 ± 0.0018; local analysis follow-up $K_i$, 0.0069 ± 0.0019). However, it was seen that the percentage progressions within individuals sometimes varied widely between the central and local analyses. This most likely reflects a combination of differences in region placement and head tilt. The normalization process used in the central analysis allowed the same putamen region to be assessed between pairs of scans. In the local analyses, ROI placement was by inspection and head tilt between studies occasionally led to falls in putamen $^{18}$F-DOPA $K_i$ in one hemisphere and rises in the other. This was not seen after spatial normalization. The local and central analyses also differed in the programs used to generate $K_i$ data (where the local centers each used different programs and where the consistency between different analysis software is not known). The putamen $K_i$ values provided by the local analysis for the subjects identified by the central analysis as having normal imaging were, with the exception of 1 subject, all within 2 SDs of our normal mean. As with the central analysis, the local analysis did not show any significant change in putamen $K_i$ for these subjects over 2 y. However, the within-subject $K_i$ variance between baseline and follow-up imaging, from the subjects with normal scans, was on average 15% in the local analysis but only 8% in the central analysis.

**TABLE 4**
Difference in $K_i$ Decline Between Ropinirole vs. L-DOPA Groups in Striatal Subregions

| Striatal subregion | Absolute % difference in $K_i$ decline between treatment groups | Relative % difference in $K_i$ decline between treatment groups |
|---|---|---|
| Putamen | 6.86 | 33.4 |
| Caudate nucleus | 4.6 | 31.5 |
| Ventral striatum | 1.28 | 13 |

In each region, the absolute and percentage $K_i$ loss was in favor of ropinirole—that is, group mean $K_i$ decline was greater in L-DOPA group compared with that of ropinirole group. Mean scan-to-scan interval: ropinirole, 615 ± 97.7 d; L-DOPA, 613 ± 103.3 d.

## DISCUSSION

To our knowledge, this is the first study of a putative disease-modifying agent in PD where changes in $^{18}$F-DOPA PET imaging rather than clinical endpoints have formed the primary measure of drug efficacy. This study has involved far greater subject numbers (186 subjects) than previous similar investigations and allowed the potential 372 PET datasets to be acquired from 6 PET units distributed globally. PET image analysis was undertaken at a single center, providing what we have now termed a distributed acquisition/centralized analysis design. This is the first time such an approach has been used to assess a neuroimaging endpoint, and the exercise has taught us a great deal about the considerations required and difficulties inherent when undertaking this type of analysis.

Study inception to the acquisition of the last $^{18}$F-DOPA image, in this 2-y longitudinal trial, took a period of >5 y, with the design of the central analysis and subsequent $K_i$ data collection occurring only in the last 2 y of the study. Before collecting individual $K_i$ values, there was a prolonged period of consideration and pilot data examination,

culminating in development of the final analysis method (shown as a flow diagram in Fig. 5).

When combining paired image datasets from different cameras it is necessary to consider both the need to achieve good compliance and reproducibility within individual centers as well as the need to identify potential sources of bias arising. Parameters regarding image acquisition and reconstruction before data are transferred to the site performing the central analysis must be considered, as must the method of data transfer—which, in this case, involved 325 individual images—if confusion between subjects and either baseline or follow-up imaging is not to occur. When selecting a program for the application of a mathematic model to allow quantification of radiotracer uptake, it is necessary to consider its flexibility and compatibility between variously acquired and reconstructed image datasets and to have the expertise available to deal with compatibility difficulties arising. A major difficulty of a local analysis approach is that the consistency of the analysis software between centers is not known and, hence, different values and normal ranges may well exist.

In a study such as this, the rigor with which the blind identification and removal of images from which spurious results would be obtained is imperative if findings are not to be skewed and power reduced. In this article we have highlighted the importance of reviewing each individual input function curve and assessing possible head movement between early and late time frames.

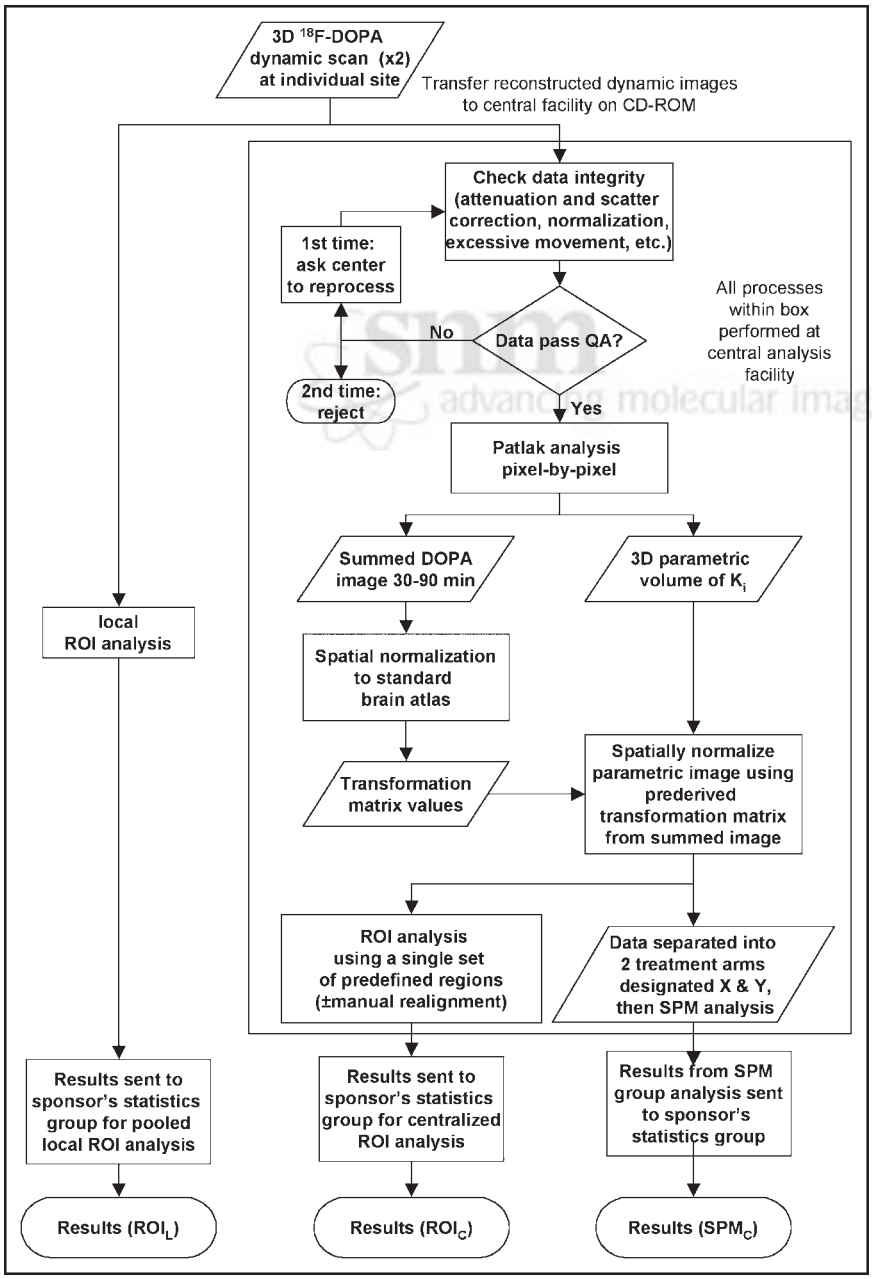


**FIGURE 5.** Flow diagram outlining various stages in this distributed acquisition/centralized analysis methodologic approach. QA = quality analysis; $ROI_L$ = local ROI analysis; $ROI_C$ = centralized ROI analysis; $SPM_C$ = centralized SPM analysis.

The manner by which target regions are identified in PET images will remain a subject of debate; however, the method we have outlined, involving placement of standard template volumes onto normalized parametric images with manual correction of ROI displacement, seems to us a sensible approach. Whether an ROI analysis or SPM is preferable is outside the scope of this article. Performance of both approaches would seem advantageous: SPM is exploratory and not based on predetermined ROIs, which may mask small focal changes within ROIs. It does, however, require a higher level of smoothing.

In all of the above, with the large number of manipulations and checks that must be made, demonstration of blindness to treatment is imperative.

Outside of the analysis method, a particular concern about using PET as a biomarker of disease progression is direct pharmacologic effects of medication on imaging parameters (*37*). It has not been directly proven that dopamine agonists or L-DOPA therapy do not independently affect $^{18}$F-DOPA uptake independent of disease progression. Two pieces of evidence from the data obtained in this study are against such a direct effect: The first is the difference in absolute and relative progression rates in $^{18}$F-DOPA $K_i$ decline between the treatment groups in the different striatal regions (Table 4). It is known that subregions of the striatal complex are differentially affected in PD (*27*), and slower $^{18}$F-DOPA uptake decline in the caudate nucleus compared with the putamen has previously been described (*4*). In this study we found that dopaminergic function in the ventral striatum declines at a significantly slower rate than in either the caudate nucleus or the putamen in early PD. We have shown that the difference in absolute and relative decline between ropinirole versus L-DOPA treatment varies between these striatal regions (Table 4). The fact that the absolute difference in decline between the 2 treatments is 6.86% in the putamen versus only 1.28% in the ventral sriatum argues against a systematic effect on $^{18}$F-DOPA uptake by either therapy alone. If this was the case, a similar difference in reduction between the treatment types across the striatum might be expected. The lack of change within the baseline normal scans in subjects receiving either treatment over 2 y is also reassuring in this regard (*6*).

## CONCLUSION

$^{18}$F-DOPA PET can been used in a distributed acquisition/centralized analysis manner to provide a biomarker of PD progression by which the efficacy of disease-modifying therapies can be judged. Such an approach permits the investigation of large numbers of patients without the need for subjects to travel extensive distances or the placement of excessive imaging burdens on a single PET center. However, there are numerous parameters that must be considered and data checks applied before such an approach can be successfully adopted and implemented.

## ACKNOWLEDGMENTS

The REAL-PET study was sponsored by GlaxoSmith-Kline. One of the authors is a Wellcome Research Clinical Training Fellow.

## REFERENCES

1. Brooks DJ. Monitoring neuroprotection and restorative therapies in Parkinson's disease with PET. *J Neural Transm Suppl*. 2000;60:125–137.
2. Brooks DJ. Imaging end points for monitoring neuroprotection in Parkinson's disease. *Ann Neurol.* 2003;53(suppl 3):S110–S119.
3. Garnett ES, Firnau G, Nahmias C. Dopamine visualized in the basal ganglia of living man. *Nature.* 1983;305:137–138.
4. Nurmi E, Ruottinen HM, Bergman J, et al. Rate of progression in Parkinson's disease: a 6-[$^{18}$F]fluoro-L-dopa PET study. *Mov Disord.* 2001;16:608–615.
5. Morrish PK, Sawle GV, Brooks DJ. An [$^{18}$F]dopa-PET and clinical study of the rate of progression in Parkinson's disease. *Brain.* 1996;119:585–591.
6. Whone AL, Watts RL, Stoessl AJ, et al. Slower progression of Parkinson's disease with ropinirole versus levodopa: the REAL-PET study. *Ann Neurol.* 2003;54:93–101.
7. Rakshi JS, Pavese N, Uema T, et al. A comparison of the progression of early Parkinson's disease in patients started on ropinirole or L-dopa: an $^{18}$F-dopa PET study. *J Neural Transm.* 2002;109:1433–1443.
8. Oertel WH, Schwarz J, Leenders KL, Hundemer HP, Lledo A, Wolters EC. Results of a three year randomised, double-blind PET controlled study of pergolide vs. L-dopa as monotherapy in early Parkinson's disease (PELMOPET-trial) [abstract]. *J Neurol Sci.* 2001;187(suppl 1):444.
9. Rutland MD. A single injection technique for subtraction of blood background in $^{131}$I-hippuran renograms. *Br J Radiol.* 1979;52:134–137.
10. Patlak CS, Blasberg RG, Fenstermacher JD. Graphical evaluation of blood-to-brain transfer constants from multiple-time uptake data. *J Cereb Blood Flow Metab.* 1983;3:1–7.
11. Spinks TJ, Jones T, Bloomfield PM, et al. Physical characteristics of the ECAT EXACT 3D positron tomograph. *Phys Med Biol.* 2000;45:2601–2618.
12. Adam LE, Zaers H, Ostertag H, Trojan H, Bellemann ME, Brix G. Performance evaluation of the whole-body PET scanner ECAT EXACT HR+ following the IEC standard. *IEEE Trans Nucl Sci.* 1997;NS-44:1172–1179.
13. Wienhard K, Eriksson L, Grootoonk S, Casey M, Pietrzyk U, Heiss WD. Performance evaluation of the positron scanner ECAT EXACT. *J Comput Assist Tomogr.* 1992;16:804–813.
14. Bailey DL. 3D acquisition and reconstruction in positron emission tomography. *Ann Nucl Med.* 1992;6:123–130.
15. Bailey DL, Young HE, Bloomfield PM, et al. A continuously rotating PET camera: performance characteristics, comparison with a full ring system, initial clinical studies, and installation considerations in a nuclear medicine department. *Eur J Nucl Med.* 1997;24:6–15.
16. Ceravolo R, Piccini P, Bailey DL, Jorga KM, Bryson H, Brooks DJ. $^{18}$F-DOPA PET evidence that tolcapone acts as a central COMT inhibitor in Parkinson's disease. *Synapse.* 2002;43:201–207.
17. Turjanski N, Lees AJ, Brooks DJ. Striatal dopaminergic receptor dysfunction in patients with restless legs syndrome: $^{18}$F-dopa and $^{11}$C-raclopride PET studies. *Neurology.* 1999;52:932–937.
18. Hoffman JM, Melega WP, Hawk TC, et al. The effects of carbidopa administration on 6-[$^{18}$F]fluoro-L-dopa kinetics in positron emission tomography. *J Nucl Med.* 1992;33:1472–1477.
19. Sawle GV, Burn DJ, Morrish PK, et al. The effect of entacapone (OR-611) on brain [$^{18}$F]-6-L-fluorodopa metabolism: implications for levodopa therapy of Parkinson's disease. *Neurology.* 1994;44:1292–1297.
20. Townsend D, Spinks T, Jones T, et al. Aspects of three dimensional reconstruction for a multi ring positron tomograph. *Eur J Nucl Med.* 1989;15:741–745.
21. Kinahan PE, Rogers GJ. Analytic 3-D image reconstruction using all detected events. *IEEE Trans Nucl Sci.* 1989;NS-36:964–968.
22. Watson CC, Newport D, Casey ME. A single scatter simulation technique for scatter correction in 3D PET. In: Grangeat P, Amans J-L, eds. *Three-Dimensional Image Reconstruction in Radiology and Nuclear Medicine.* Vol. 4. Dordrecht, The Netherlands: Kluwer Academic; 1996:255–268.
23. Ollinger JM. Model-based scatter correction for fully 3D PET. *Phys Med Biol.* 1996;41:153–176.

24. Rakshi J, Bailey DL, Morrish PK, Brooks DJ. Implementation of 3D acquisition, reconstruction and analysis of dynamic fluorodopa studies. In: Myers R, Cunningham VJ, Bailey DL, Jones T, eds. *Quantification of Brain Function Using PET*. San Diego, CA: Academic Press; 1996:82–87.
25. Moore RY, Whone AL, McGowan S, Brooks DJ. Monoamine neuron innervation of the normal human brain: an $^{18}$F-DOPA PET study. *Brain Res.* 2003;982:137–145.
26. Whone AL, Moore RY, Piccini PP, Brooks DJ. Plasticity of the nigropallidal pathway in Parkinson's disease. *Ann Neurol.* 2003;53:206–213.
27. Kish SJ, Shannak K, Hornykiewicz O. Uneven pattern of dopamine loss in the striatum of patients with idiopathic Parkinson's disease. pathophysiologic and clinical implications. *N Engl J Med.* 1988;318:876–880.
28. Morrish PK, Sawle GV, Brooks DJ. Regional changes in [$^{18}$F]dopa metabolism in the striatum in Parkinson's disease. *Brain.* 1996;119:2097–2103.
29. Statistical Parametric Mapping: SPM99. Functional Imaging Laboratory, Institute of Neurology, London, U.K. Available at: http://www.fil.ion.ucl.ac.uk/spm/spm99.html. Accessed April 30, 2004.
30. Evans AC, Marrett S, Neelin P, et al. Anatomical mapping of functional activation in stereotactic coordinate space. *Neuroimage.* 1992;1:43–53.
31. Seibyl JP, Jennings D, Tabamo R, Marek K. Dopamine transporter imaging in Parkinson's disease patients in long-term neuroprotective trials: a role for imaging in trial recruitment [abstract]? *J Nucl Med.* 2003;44(suppl):118P
32. Friston KJ, Holmes AP, Worsley KJ, Poline JB, Frith CD, Frackowiak RSJ. Statistical parametric maps in functional imaging: a general linear approach. *Hum Brain Mapp.* 1995;2:189–210.
33. Ito K, Morrish PK, Rakshi JS, et al. Statistical parametric mapping with $^{18}$F-dopa PET shows bilaterally reduced striatal and nigral dopaminergic function in early Parkinson's disease. *J Neurol Neurosurg Psychiatry.* 1999;66:754–758.
34. Rakshi JS, Uema T, Ito K, et al. Frontal, midbrain and striatal dopaminergic function in early and advanced Parkinson's disease: a 3D [$^{18}$F]dopa-PET study. *Brain.* 1999;122:1637–1650.
35. Ito K, Nagano-Saito A, Kato T, et al. Striatal and extrastriatal dysfunction in Parkinson's disease with dementia: a 6-[$^{18}$F]fluoro-L-dopa PET study. *Brain.* 2002;125:1358–1365.
36. Poline JB, Worsley KJ, Holmes AP, et al. Estimating smoothness in statistical parametric maps: variability of p values. *J Comput Assist Tomogr.* 1995;19:788–796.
37. Ahlskog JE. Slowing Parkinson's disease progression: recent dopamine agonist trials. *Neurology.* 2003;60:381–389.

JNM The Journal of NUCLEAR MEDICINE

# A Technique for Standardized Central Analysis of 6-$^{18}$F-Fluoro-l-DOPA PET Data from a Multicenter Study

Alan L. Whone, Dale L. Bailey, Philippe Remy, Nicola Pavese and David J. Brooks

*J Nucl Med.* 2004;45:1135-1145.



*The Journal of Nuclear Medicine* is published monthly.
SNMMI | Society of Nuclear Medicine and Molecular Imaging
1850 Samuel Morse Drive, Reston, VA 20190.
(Print ISSN: 0161-5505, Online ISSN: 2159-662X)



SNMMI SOCIETY OF NUCLEAR MEDICINE AND MOLECULAR IMAGING